Supplementary Materials for

Capturing Metastable Electrocatalytic Active Structures With Atomic Resolution

Zixiao Shi[1*]†, Qihao Li[1]†, Andres Molina Villarino[1], Michael Colletta[2], Noah Schnitzer[3,4], Dasol Yoon[3], Mihail Krumov[1], Christopher J. Pollock[5], Guanxing Li[2,4], Yimo Han[6*], Héctor D. Abruña[1*], David A. Muller[2,4*]

[1] *Department of Chemistry and Chemical Biology, Cornell University, Ithaca, New York 14853, USA*

[2] *School of Applied and Engineering Physics, Cornell University, Ithaca, NY 14853, USA.*
[3] *Department of Materials Science and Engineering, Cornell University, Ithaca, New York 14853, USA*

[4] *Kavli Institute at Cornell for Nanoscale Science, Ithaca, NY 14853, USA.*

[5] *Cornell High Energy Synchrotron Source, Wilson Laboratory, Cornell University, Ithaca, NY 14853, USA,*

[6] *Department of Materials Science and Nanoengineering, Rice University, Houston, TX 77006, USA*

†These authors contributed equally to this work

Corresponding author:
zs353@cornell.edu
yh76@rice.edu
hda1@cornell.edu
david.a.muller@cornell.edu

Contents

Abbreviations

Name and crystal phases of samples

$Ni(OH)_2$: β-phase nickel hydroxide, where Ni exists as Ni^{2+}.[1]

NiOOH: γ-phase nickel oxyhydroxide, no single crystal data for this material is available. Ni exists with an average oxidation state of $Ni^{3.67+}$. Water molecules and anions/cations are intercalated between the layers, and the position/ratio of H is unknown. The full formula can be written as $NiOOH_x$ $(A,B)_y$, where A are K^+, CO_3^{2-} and B are water molecules. [1].

$NiFe(OH)_2$: Nickel iron hydroxides, also referred to as nickel iron layered double hydroxides (NiFe LDHs). No single crystal data is available, the crystal structure resembles that of α-phase nickel hydroxides. Ni exists as Ni^{2+} and Fe as Fe^{3+}. Water molecules and anions are intercalated between the layers; the anions are primarily CO_3^{2-} (due to the synthesis conditions), balancing the extra positive charge introduced by Fe^{3+}. The full formula can be written as $Ni_{1-x}Fe_x(OH)_2(CO_3)_{x/2}\cdot yH_2O$ [2–4], in our synthesis, x = 0.2.

NiFeOOH: Nickel iron oxyhydroxides. No single crystal data is available, the crystal structure resembles that of γ-phase nickel oxyhydroxide. The valence of Ni and Fe vary between $Ni^{3+/4+}$ and $Fe^{3+/4+}$ depending on synthesis conditions and reports. In our case, Ni exists as $Ni^{3.4+}$ and Fe as $Fe^{3.2+}$. Water molecules and anions/cations are intercalated between the layers, and the position/ratio of H is unknown. The full formula can be written as $Ni_{1-x}Fe_xOOH_y$ $(A,B)_z$, where A are K^+, CO_3^{2-} and B are water molecules, x = 0.2.

$Ni(OH)_2$@FeOOH: β-phase nickel hydroxide with δ-phase iron oxyhydroxide selectively grown on the edge planes of the β-$Ni(OH)_2$. Ni exists as Ni^{2+}, and Fe exists as Fe^{3+}. In our synthesis, Fe is a 2% molar ratio in all metal sites.

All structures were characterized using scanning transmission electron microscopy (STEM) imaging, electron diffraction, and X-ray diffraction (XRD).

Name of characterization techniques

STEM: scanning transmission electron microscopy
Cryo-STEM: cryogenic scanning transmission electron microscopy
HAADF: high-angle annular dark field
iDPC: Integrated differential phase contrast
EELS: electron energy loss spectroscopy
SEND: scanning electron nanobeam diffraction
SEM: scanning electron microscopy
XRD: X-ray diffraction
XAS: X-ray absorption spectroscopy
XANES: X-ray absorption near-edge structure
EXAFS: extended X-ray absorption fine structure
FT-EXAFS: Fourier transformed extended X-ray absorption fine structure
FFT: fast Fourier transform
CV: Cyclic Voltammetry

Supplementary Figure

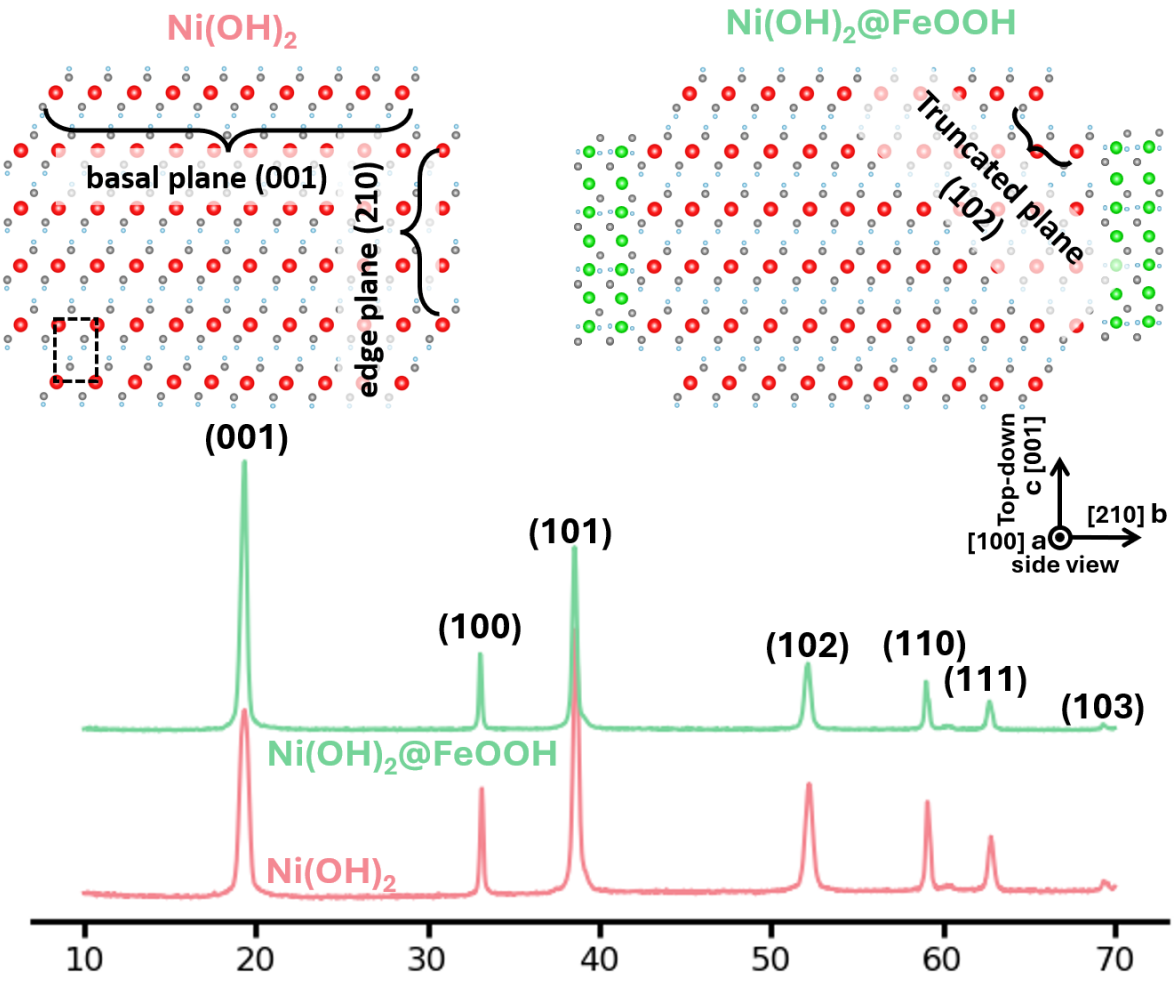

Fig. S1. XRD pattern of $Ni(OH)_2$ and $Ni(OH)_2$@FeOOH
Both XRD patterns of $Ni(OH)_2$ and $Ni(OH)_2$@FeOOH match the crystal structure of β-$Ni(OH)_2$, and no peak of any phase of FeOOH is observed. The above atomic structure of $Ni(OH)_2$ and $Ni(OH)_2$@FeOOH is built based on the latter atomic resolution STEM imaging results.

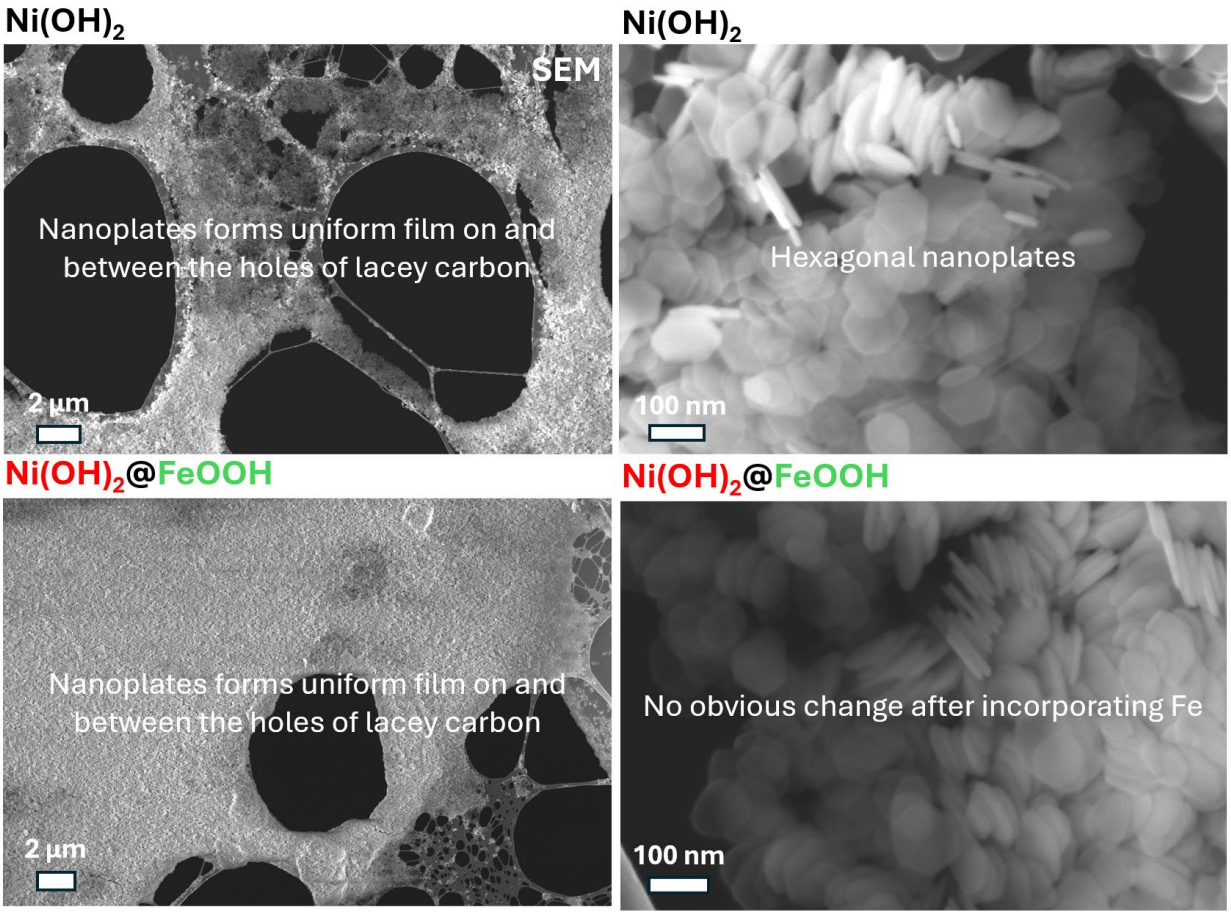

Fig. S2. SEM images of $Ni(OH)_2$ and $Ni(OH)_2$@FeOOH

The SEM images of $Ni(OH)_2$ nanoplates shows the uniform geometric distribution of the nanoplate on lacey carbon TEM grid. The Zoom in SEM image show the uniform shape and size of the $Ni(OH)_2$ nanoplates. After post-incorporating Fe to $Ni(OH)_2$ as $Ni(OH)_2$@FeOOH, the uniform distribution and shape of $Ni(OH)_2$@FeOOH nanoplates remains. No obvious structure change of $Ni(OH)_2$@FeOOH compared to $Ni(OH)_2$ can be observed by SEM.

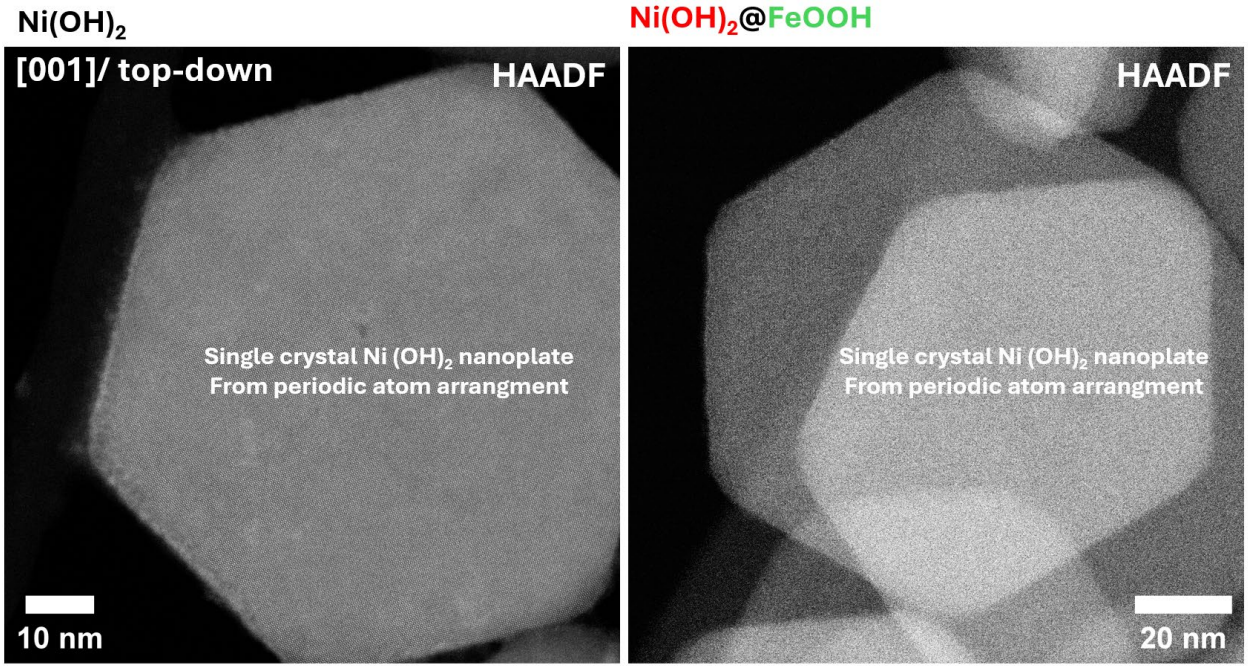

Fig. S3 STEM HAADF images of $Ni(OH)_2$ and $Ni(OH)_2$@FeOOH showing the single crystal nature of $Ni(OH)_2$

STEM HAADF images of $Ni(OH)_2$ and $Ni(OH)_2$@FeOOH from top-down views. The continuous Ni atom arrays in $Ni(OH)_2$ and $Ni(OH)_2$@FeOOH show that the single-crystal nature of $Ni(OH)_2$.

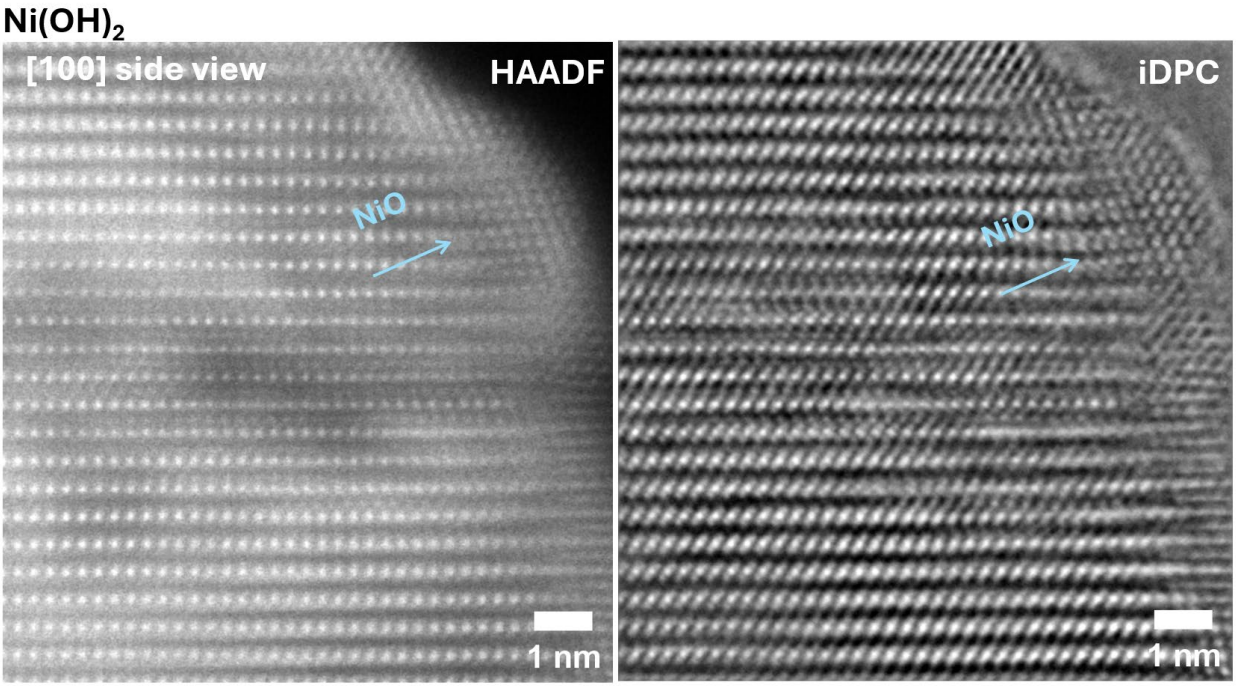

Fig. S4 STEM HAADF and iDPC of $Ni(OH)_2$ along [100] side view showing the dehydrated NiO on the surface

STEM HAADF and iDPC images of $Ni(OH)_2$, along side view, show 2D layer structure of $Ni(OH)_2$, the surface layer is NiO according to its crystal structure, meaning that $Ni(OH)_2$ dehydrated to NiO on the surface.

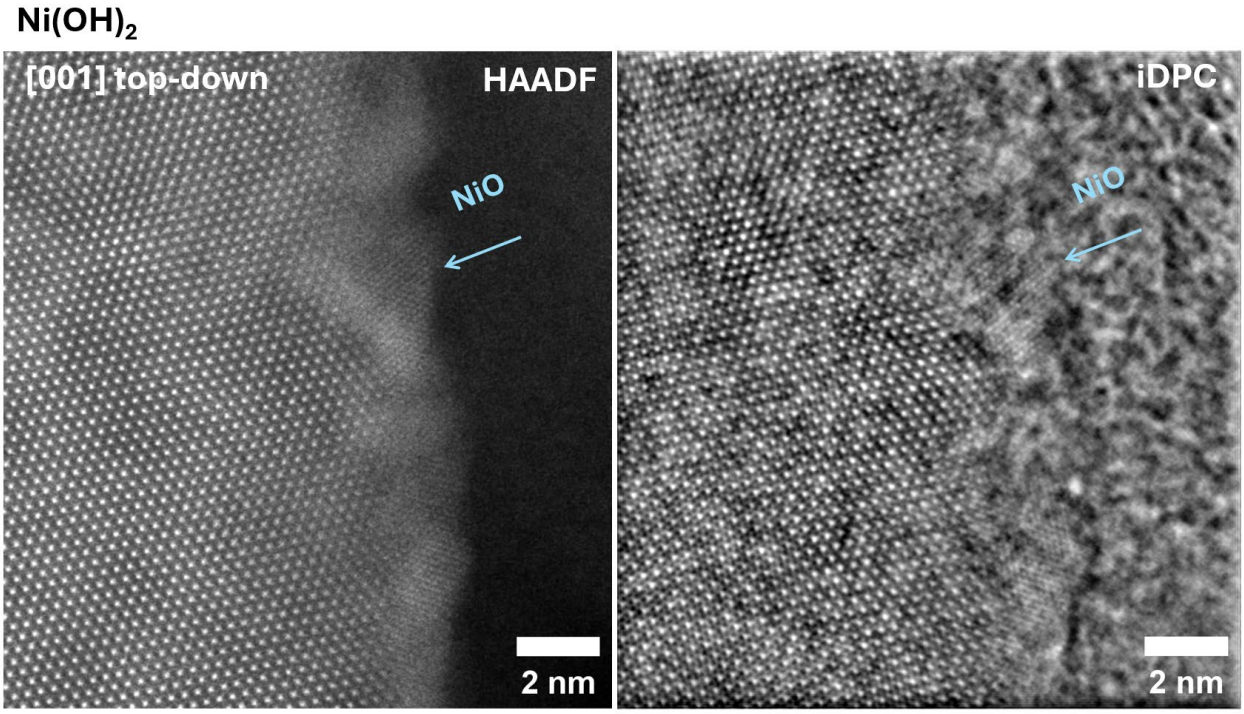

Fig. S5 STEM HAADF and iDPC of $Ni(OH)_2$ along [001] top-down view showing the dehydrated NiO on the surface

STEM HAADF and iDPC images of $Ni(OH)_2$ along the top-down view show a hexagonal structure of $Ni(OH)_2$, the surface layer is NiO according to its crystal structure, meaning that $Ni(OH)_2$ dehydrates to NiO on the surface.

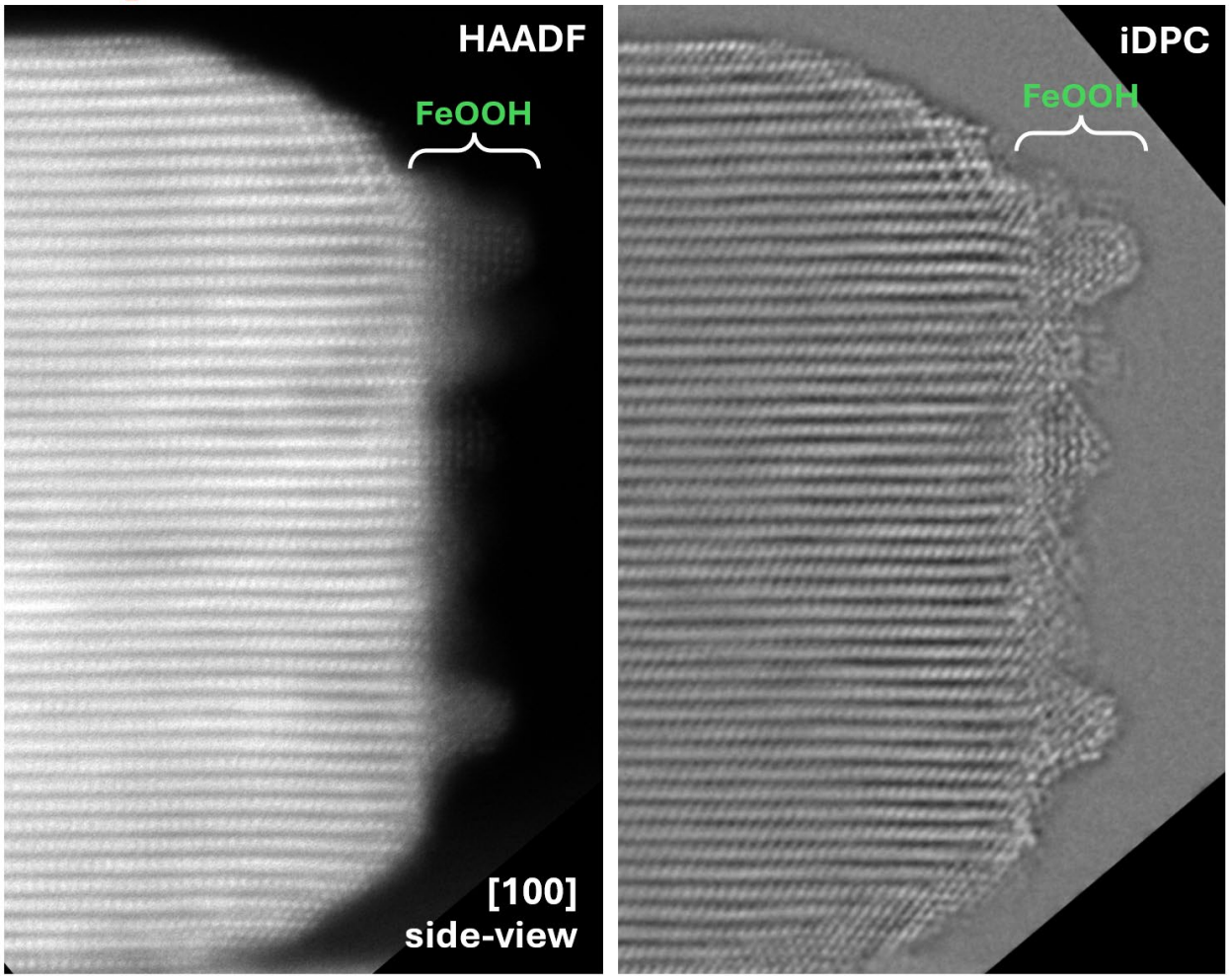

Fig. S6 STEM HAADF and iDPC of $Ni(OH)_2$@FeOOH along [100] side view showing FeOOH selectively covers the edge plane of $Ni(OH)_2$

STEM HAADF and iDPC of $Ni(OH)_2$@FeOOH along [100] side view showing δ-FeOOH selectively covers the edge plane of β-$Ni(OH)_2$.

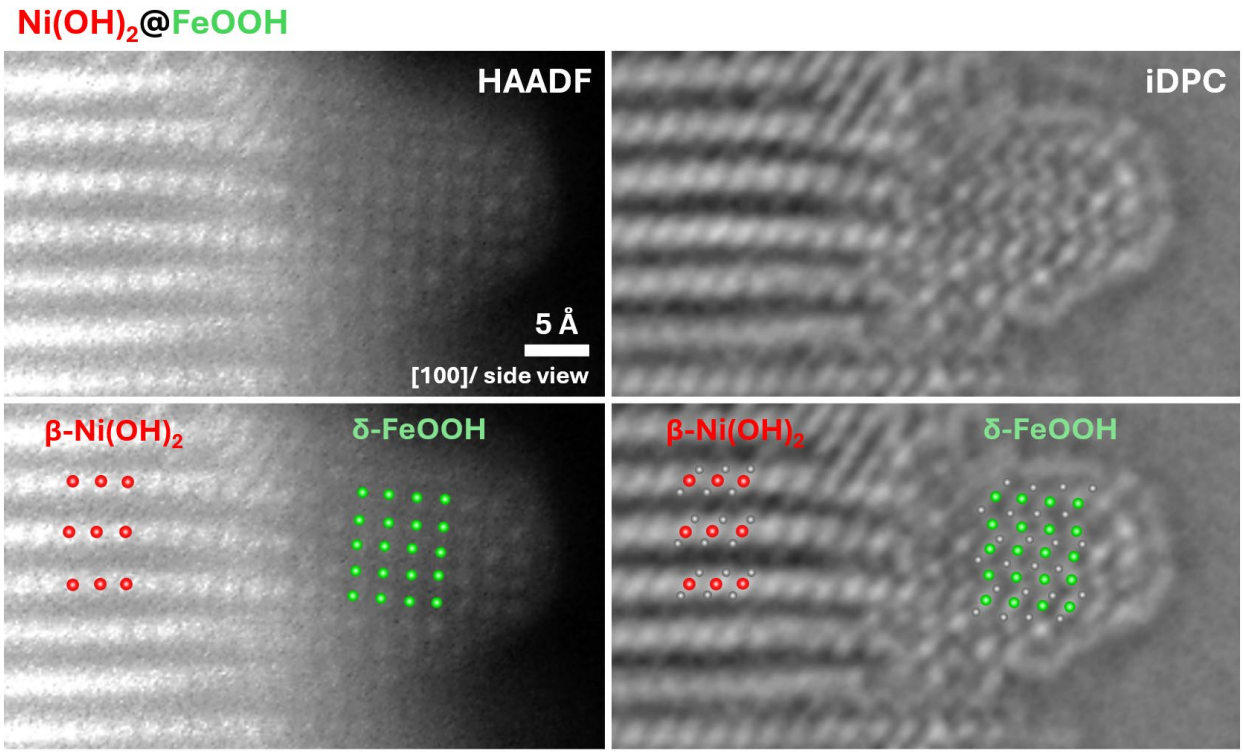

Fig. S7 STEM HAADF and iDPC zoom in image of $Ni(OH)_2$@FeOOH along [100] side view showing the surface and interface of β-$Ni(OH)_2$/δ-FeOOH

STEM HAADF and iDPC of $Ni(OH)_2$@FeOOH along [100] side view showing how the δ-FeOOH epitaxially grows on the edge plane of β-$Ni(OH)_2$, with the Fe layer growing along the Ni layer.

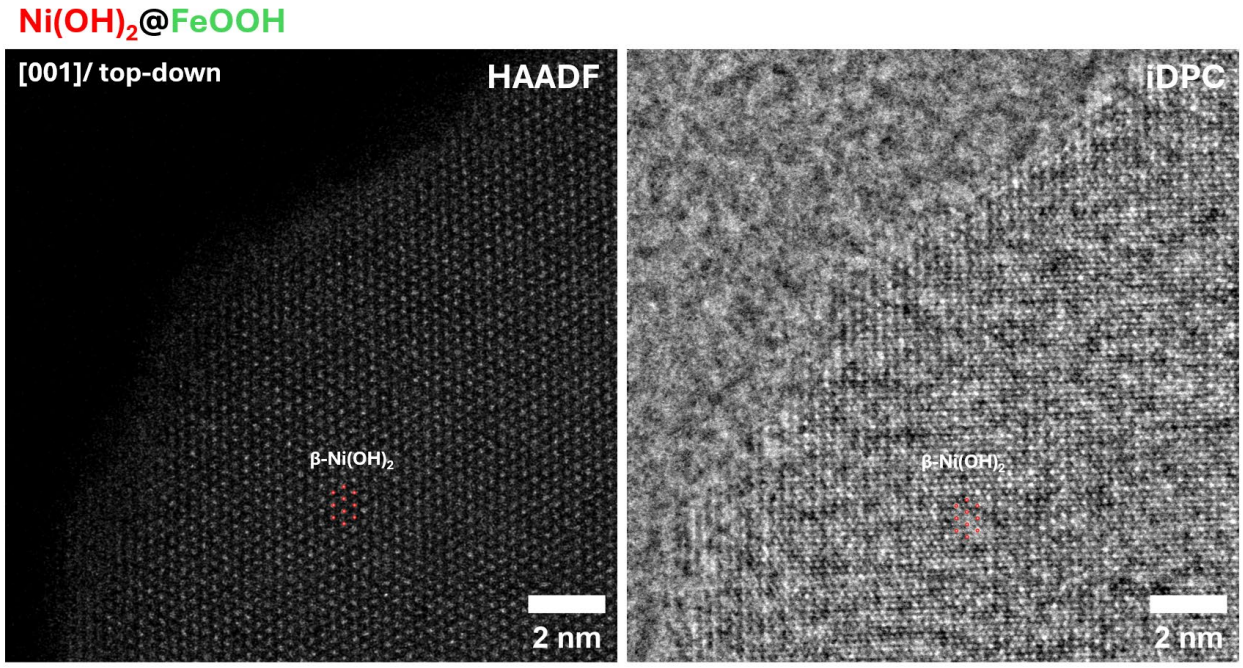

Fig. S8 STEM HAADF and iDPC of $Ni(OH)_2$@FeOOH along top-down view

STEM HAADF and iDPC of $Ni(OH)_2$@FeOOH along top-down view. We can confirm the structure of β-$Ni(OH)_2$ from the structure in that each Ni atom is surrounded by six O atoms. From a top-down view, the β-$Ni(OH)_2$ and δ-FeOOH have a hexagonal structure with similar lattice parameters, it's hard to locate where the δ-FeOOH is based on an atomic resolution image.

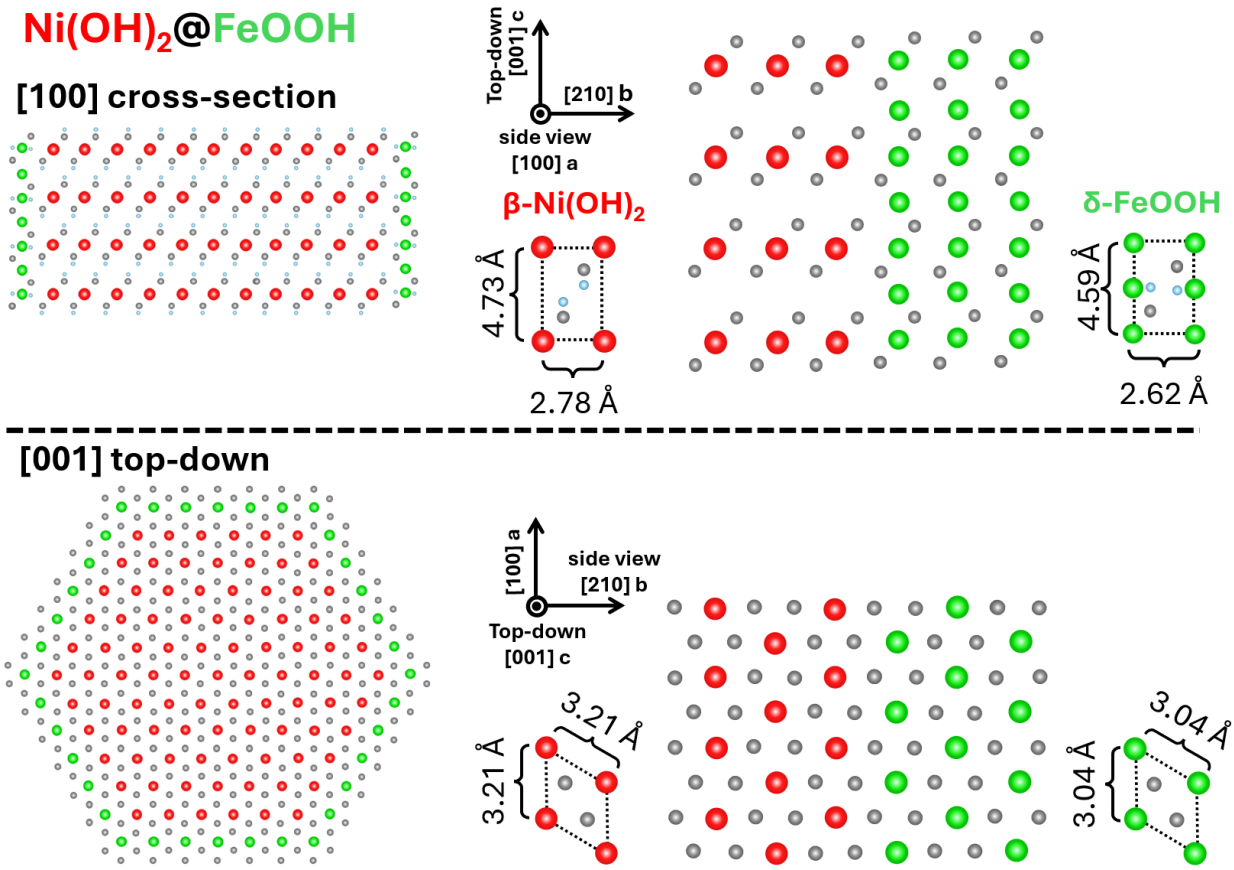

Fig. S9 Schematic atomic model of β-Ni(OH)$_2$ and δ-FeOOH in Ni(OH)$_2$@FeOOH
Schematic representations of β-Ni(OH)$_2$ and δ-FeOOH in the Ni(OH)$_2$@FeOOH heterostructure [5], shown along the [100] side view and the [001] top-down view. While δ-FeOOH does not form well-defined single crystals, we use its widely accepted hexagonal structural model for this illustration. The c-axis lattice parameter of β-Ni(OH)$_2$ (c = 4.73 Å, a/b = 3.21 Å) is 3.0% larger than that of δ-FeOOH (c = 4.59 Å, a/b = 3.04 Å), while the a/b-axis lattice parameters are 5.6% larger. Given that both materials adopt a hexagonal crystal structure and the lattice mismatch remains within the range tolerable for epitaxy, δ-FeOOH can grow epitaxially on β-Ni(OH)$_2$. However, the mismatch imposes significant tensile strain on δ-FeOOH along both the c and a/b directions, leading to its confinement into small nanoislands during growth [6].

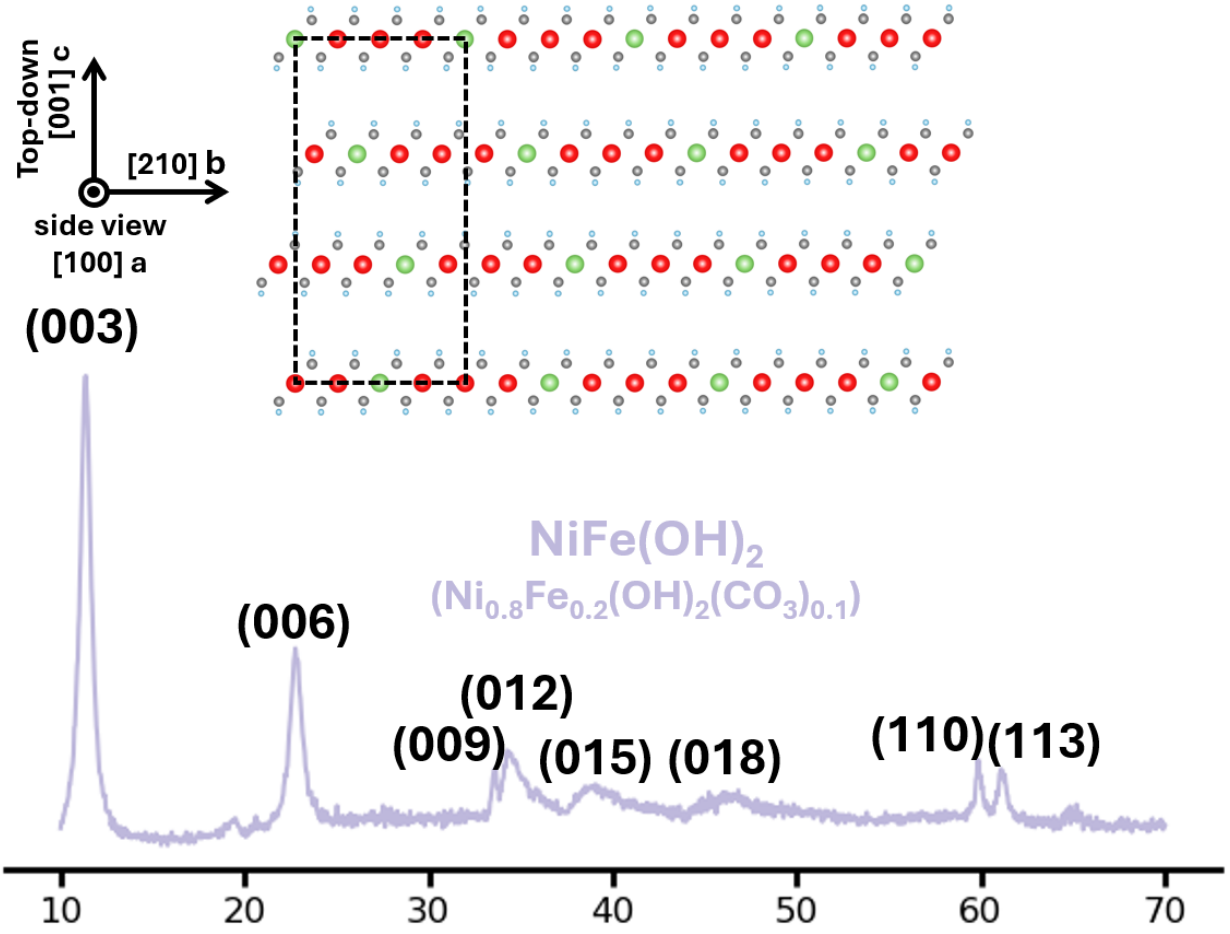

Fig. S10 XRD pattern of $NiFe(OH)_2$

X-ray diffraction (XRD) pattern of $NiFe(OH)_2$ with a 20% Fe-to-Ni mass ratio shows a strong match with the pattern of α-$Ni(OH)_2$, indicating successful incorporation of Fe into the $Ni(OH)_2$ lattice. This confirms the formation of NiFe layered double hydroxides (LDHs), featuring interlayer water molecules and anions as expected from our synthesis method. Although single-crystal data are not available for either NiFe LDHs or α-$Ni(OH)_2$ in the literature, their XRD patterns closely resemble those of MgAl LDHs, which do have well-established single-crystal structures. [7].

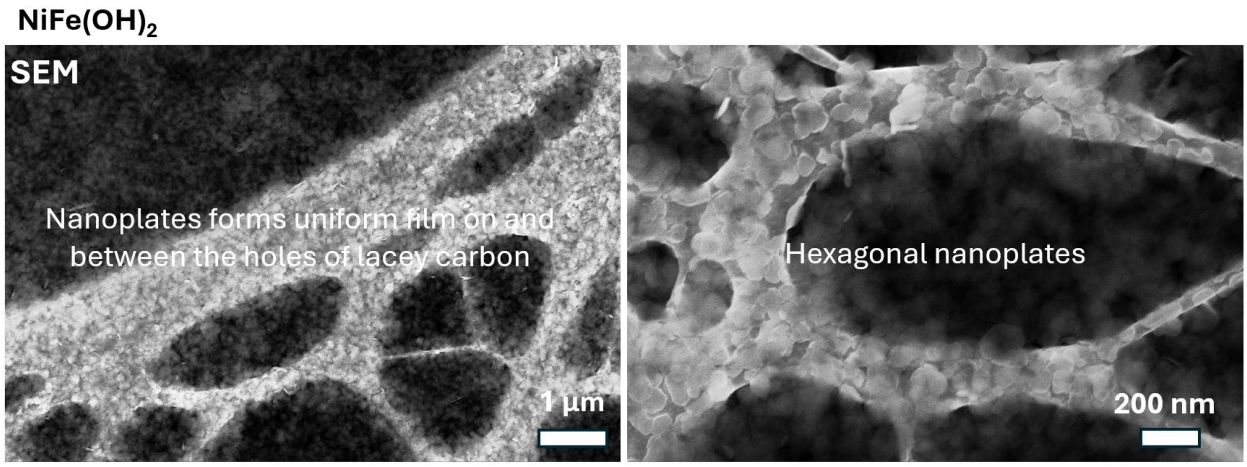

Fig. S11 SEM images of $NiFe(OH)_2$

The SEM images of $NiFe(OH)_2$ nanoplates shows the uniform geometric distribution of the nanoplate on lacey carbon TEM grid. The Zoom in SEM image show the uniform shape and size of the $NiFe(OH)_2$ nanoplates, the diameter of $NiFe(OH)_2$ is around 80 nm, smaller than 100 nm of $Ni(OH)_2$.

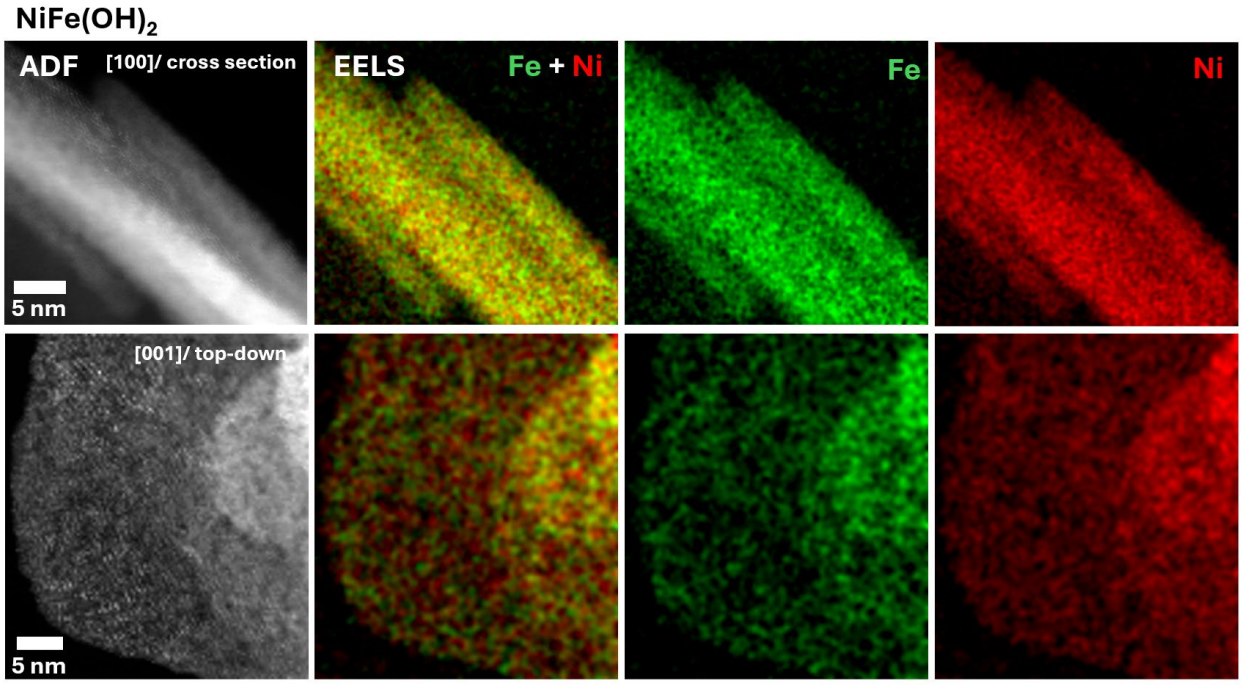

Fig. S12 STEM HAADF images and EELS mapping of $NiFe(OH)_2$

STEM EELS mapping of Ni and Fe and simultaneous ADF in $NiFe(OH)_2$ along both [100] side and [001] top-down view, showing that the Ni and Fe are homogenously distributed within the statistical noise fluctuations in $NiFe(OH)_2$ nanoplates.

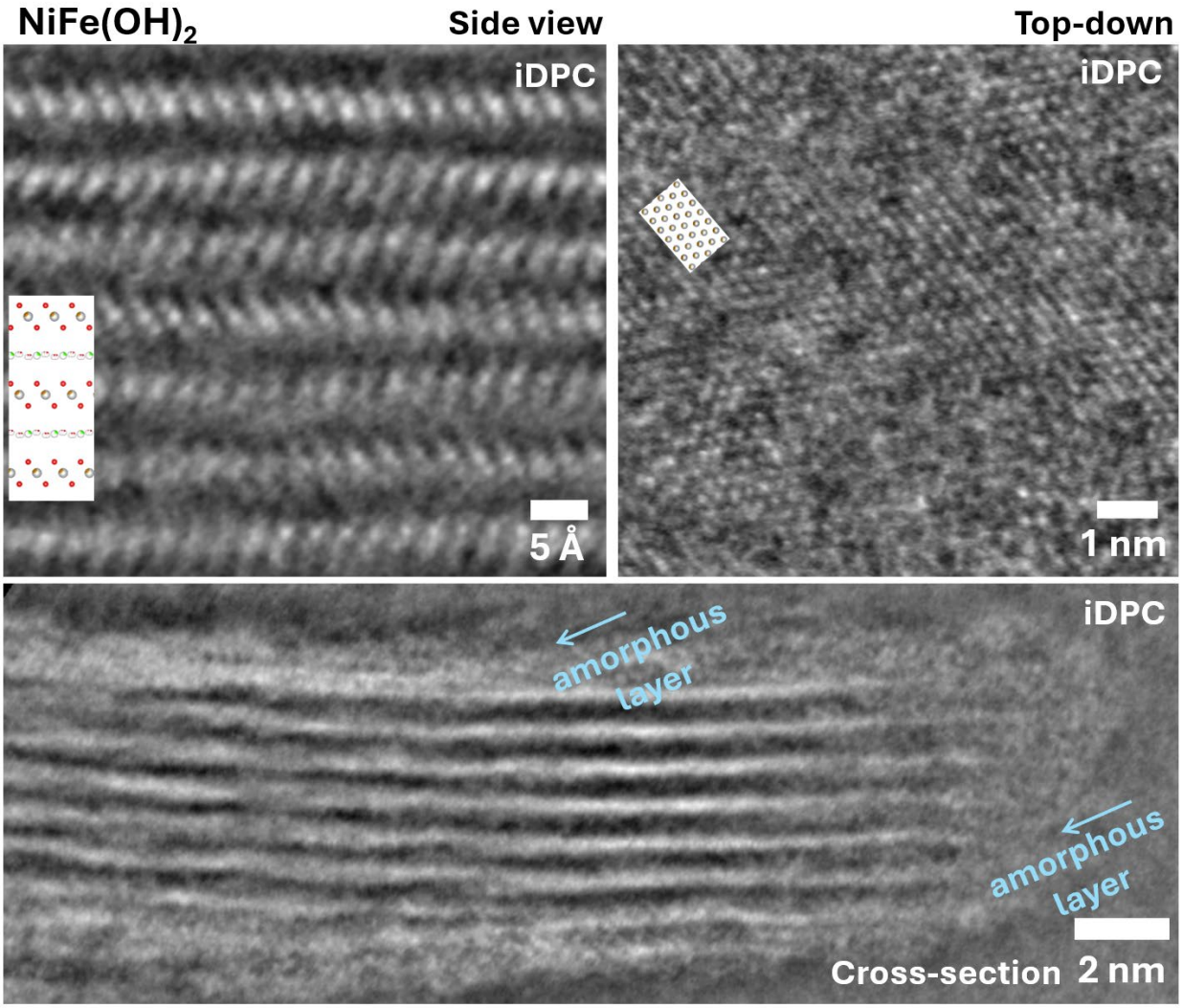

Fig. S13 STEM iDPC image of $NiFe(OH)_2$

Atomic resolution STEM iDPC images of $NiFe(OH)_2$ along [100] side and [001] top-down views. These images show that $NiFe(OH)_2$ has the crystal structure of NiFe LDHs. Noticing from the atomic resolution image along [100] side views that some of the NiFe layer has flipped its orientation, and the mistilt in top-down view, meaning the crystal structure of $NiFe(OH)_2$ is highly disordered. The surface of $NiFe(OH)_2$ is also dehydrated with a 1 nm amorphous layer on the surface.

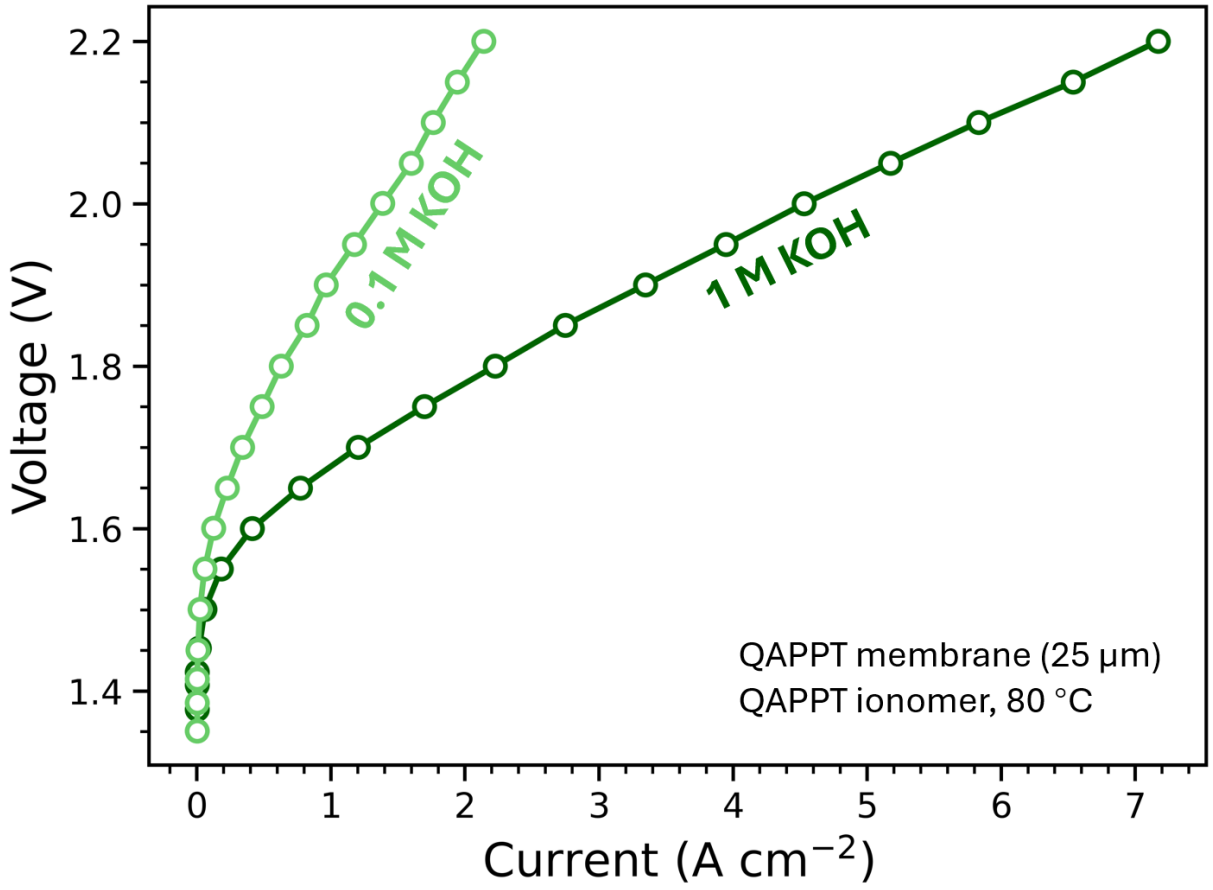

Fig. S14 Anion Exchange Membrane Water Electrolyer Performance Testing
Anion exchange membrane water electrolyzer (AEMWE) performance of the $Ni(OH)_2$@FeOOH catalysts tested at 80 °C with 1 M KOH supplied from the anode side. Cell voltage as a function of current density for MEAs fabricated with a QAPPT membrane (25 µm) and QAPPT ionomer at 80 °C, measured in 1 M KOH (dark green) and 0.1 M KOH (light green). Lines are guides to the eye; symbols are measured data points.

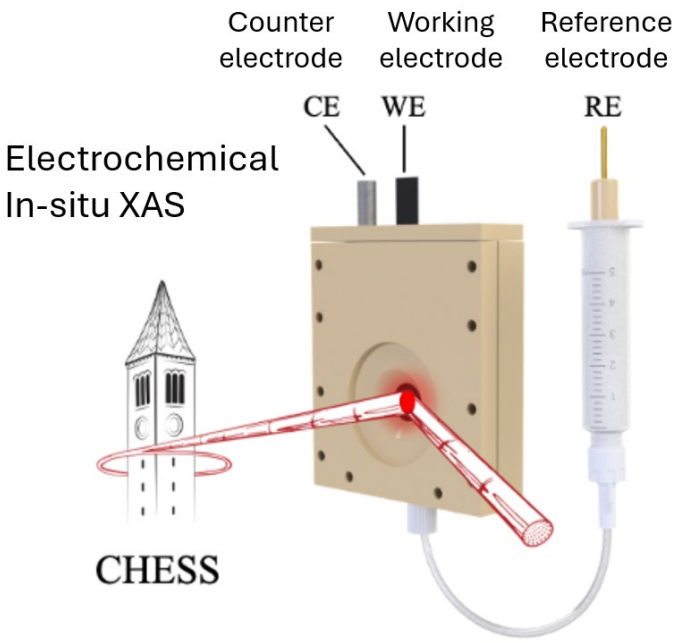

Fig. S15. Set up of electrochemical in-situ XAS
Schematic figure of electrochemical in-situ XAS measurement at Cornell High Energy Synchrotron Source (CHESS) with a graphite carbon rod as counter electrode, electrocatalysts on carbon fiber as working electrode, and Reversible Hydrogen Electrode (RHE) as reference electrode. This setup ensures that the potential applied to the electrocatalyst is close to that of RDE.

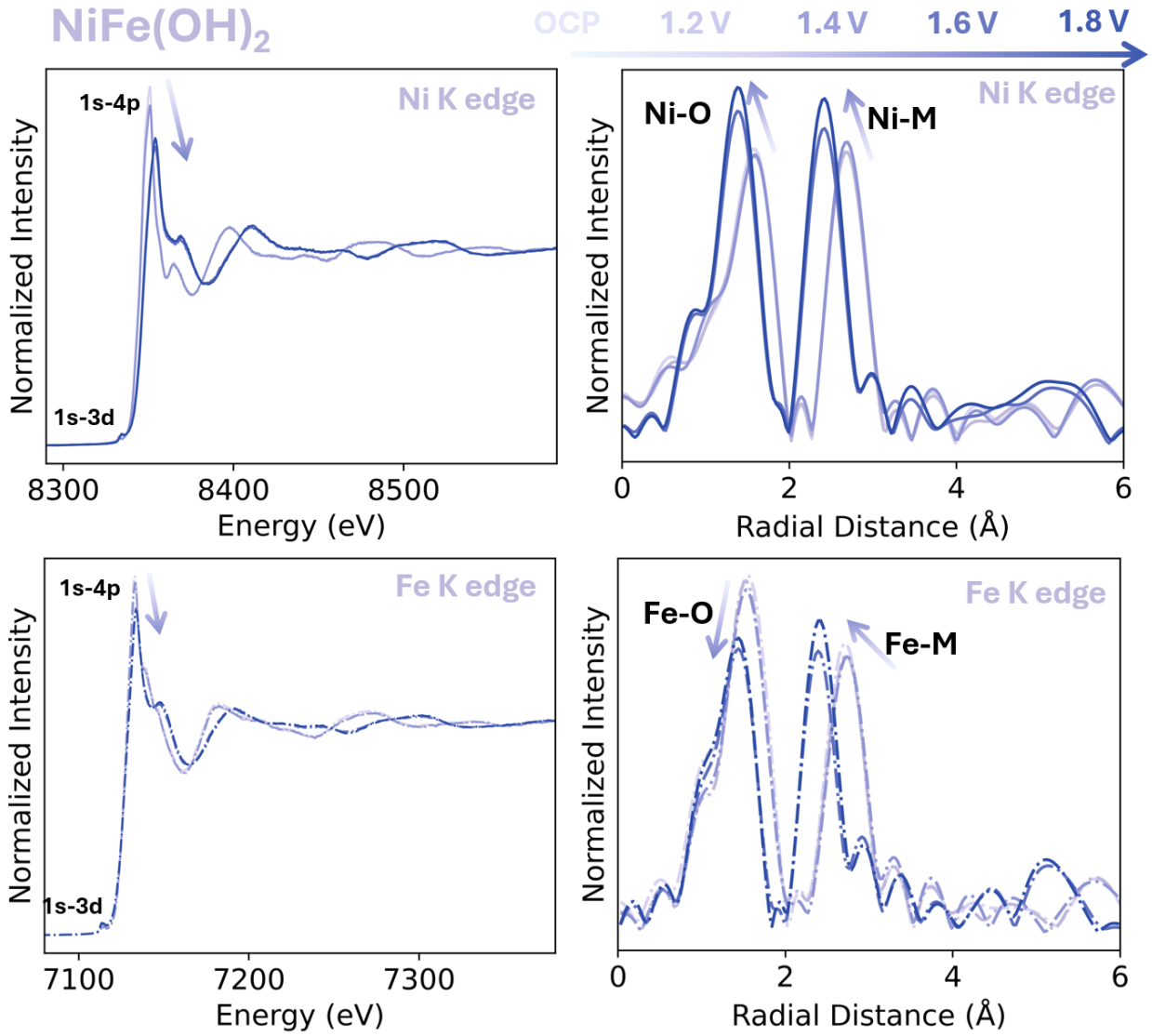

Fig. S16 electrochemical in-situ XANES and FT-EXAFS of $NiFe(OH)_2$

Electrochemical in-situ EXAFS and its FFT of $NiFe(OH)_2$ Ni K edge and Fe K edge from open circuit potential (OCP) to 1.8V vs. RHE, the right shift of 1s-4p peak in both Ni and Fe K edge is obvious in EXAFS as the potential goes higher. In the FFT of EXAFS, the Ni-Ni and Ni-O bonds have a left shift, meaning the shortening of Ni-Ni and Ni-O bonds from the β-$Ni(OH)_2$ phase to the γ-NiOOH phase at high OER potentials. The shape of the Fe K edge in the FFT of EXAFS and the shift of Fe-M, Fe-O bonds match those of Ni, meaning Fe incorporates into $Ni(OH)_2$ lattice, and changes correspondingly as β-$Ni(OH)_2$ phase to γ-NiOOH phase at high OER potentials.

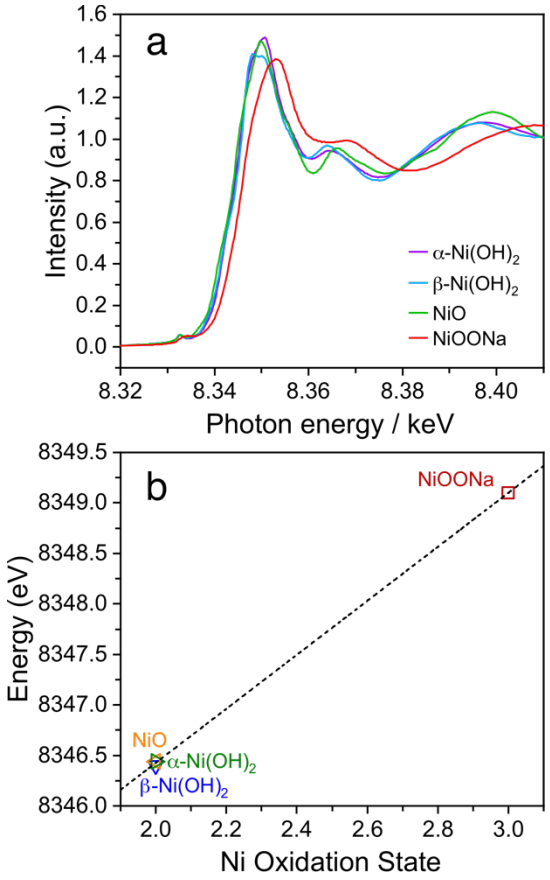

Fig. S17 Determination of Ni oxidation state by references in XAS data

(a) Ni K-edge XANES spectra of reference nickel samples, including NiO, NiOONa, α-$Ni(OH)_2$, and β-$Ni(OH)_2$. (b) Corresponding correlation between Ni K-edge energy and the average Ni oxidation states.

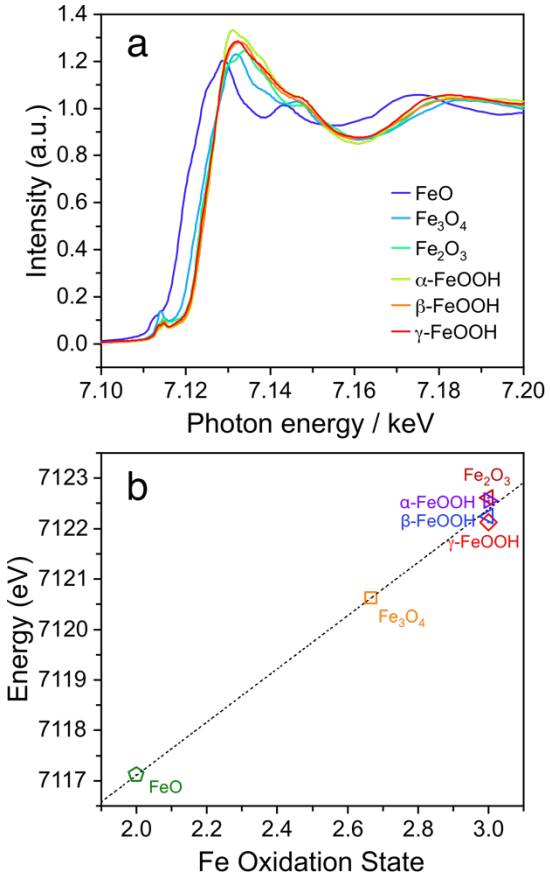

Fig. S18 Determination of Fe oxidation state by references in XAS data

(a) Fe K-edge XANES spectra of reference iron samples, including FeO, Fe_3O_4, Fe_2O_3, α-FeOOH, β-FeOOH, and γ-FeOOH. (b) Corresponding correlation between Fe K-edge energy and the average Fe oxidation state.

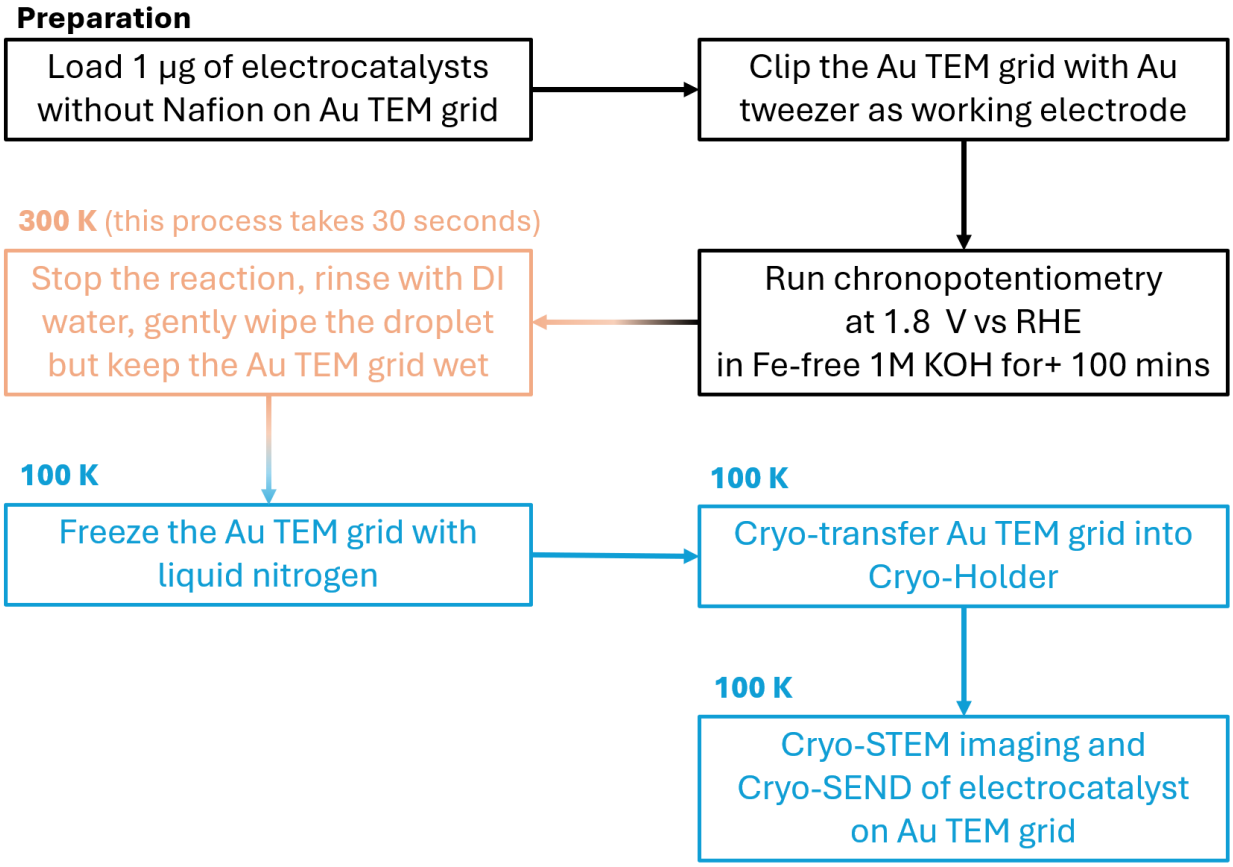

Fig. S20 Flow chart of Cryo-STEM setup

The Cryo-STEM setup can be cataloged into 3 parts: 1. The preparation of the active phase of the electrocatalyst on HexAuFoil grid. Run the OER reaction with the HexAuFoil grid at 1.8V vs RHE for 100 min to fully convert the electrocatalysts to their active phases. 2. Stop the reaction, rinse with DI water, gently wipe the droplet on the HexAuFoil grid with Kimwipe, and keep the HexAuFoil grid wet. This is the only step in which the electrocatalysts are exposed to room temperature after the reaction. 3. Freeze the HexAuFoil grid with melting solid nitrogen, cryo-transfer the frozen HexAuFoil with a Cryo-transfer holder into the electron microscope. The Cryo-STEM imaging is also at cryogenic temperature, so the whole process, the active phase of the electrocatalysts, remains.

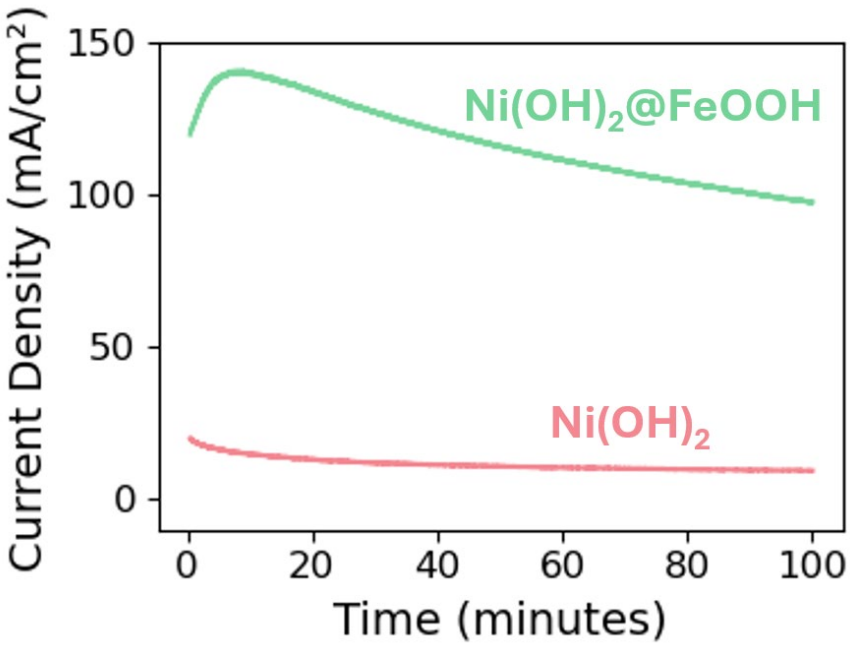

Fig. S21 Chronoamperometry of $Ni(OH)_2$ and $Ni(OH)_2$@FeOOH before Cryo-STEM
The Chronoamperometry of $Ni(OH)_2$ and $Ni(OH)_2$@FeOOH at 1.8V vs RHE before Cryo-STEM with only 1 μg of electrocatalysts on HexAuFoil grid. The $Ni(OH)_2$@FeOOH exhibits a current density of over 100 mA/cm^2 on a piece of TEM grid without any IR compensation, meaning that the $Ni(OH)_2$@FeOOH is a good electrocatalyst, and the electron conduction is very good on the HexAuFoil grid.

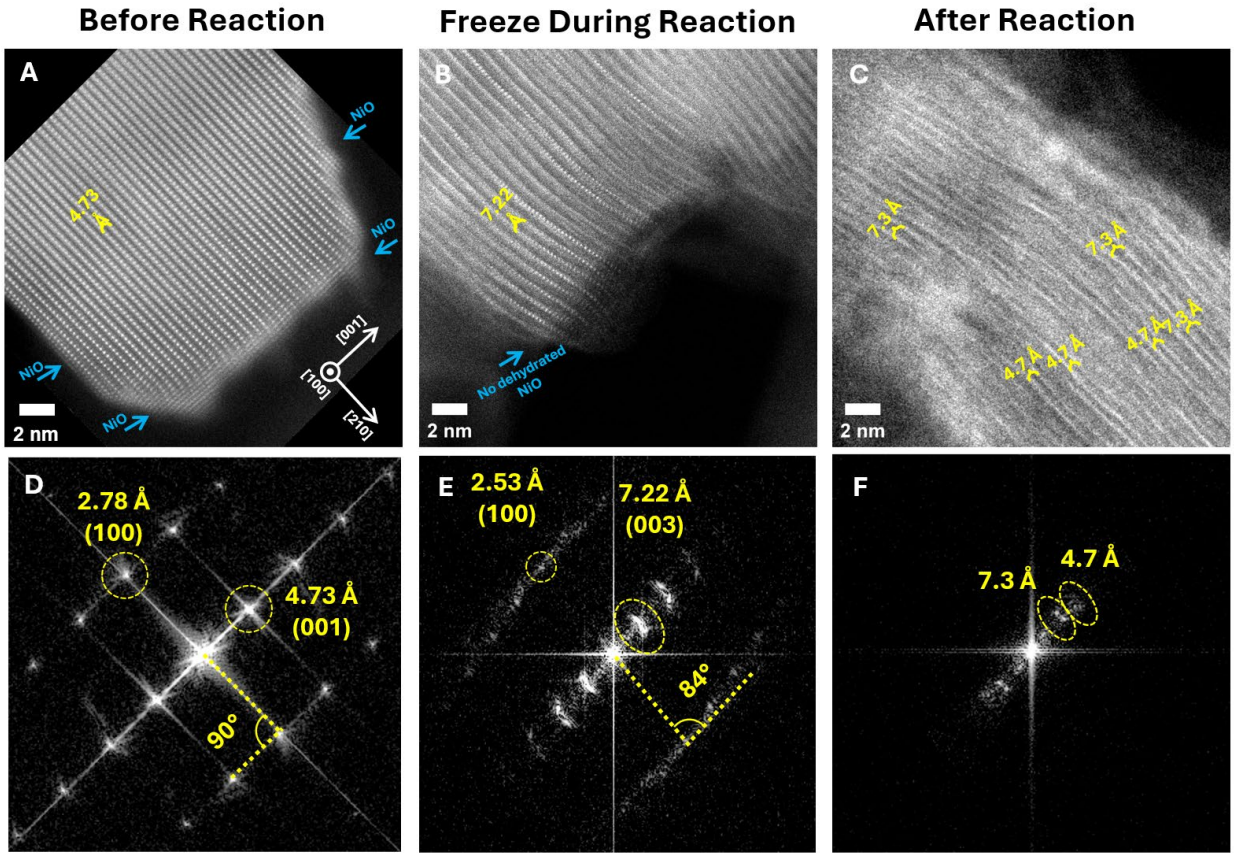

Fig. S22 Cryo-STEM HAADF images and their FFT of $Ni(OH)_2$, NiOOH, disordered $Ni(OH)_2$

(A) atomic resolution STEM-HAADF image of pristine $Ni(OH)_2$ before electrochemical testing. Fast Fourier transform (FFT) analysis confirms a 4.73 Å interlayer spacing for the (001) plane and a 2.78 Å in-plane Ni–Ni spacing along the (100) direction. Blue arrows indicate a dehydrated NiO surface layer on both basal and edge planes. (B) atomic resolution Cryo-STEM HAADF image of the active NiOOH phase, formed from $Ni(OH)_2$ under OER conditions and rapidly frozen in melting solid nitrogen to preserve its structure. The image reveals a 7.22 Å interlayer spacing for the (003) plane and a shorter 2.53 Å in-plane Ni–Ni spacing along (100). Blue arrows show a fully preserved surface without dehydration, highlighting the ability of Cryo-STEM to image the surface of the metastable structure (NiOOH). (C) HAADF image of degraded $Ni(OH)_2$, obtained by warming the NiOOH sample to room temperature after electrochemical testing. The structure shows a disordered phase with mixed interlayer spacings (4.6 Å and 7.3 Å), indicating the instability of NiOOH outside of OER or cryogenic conditions.

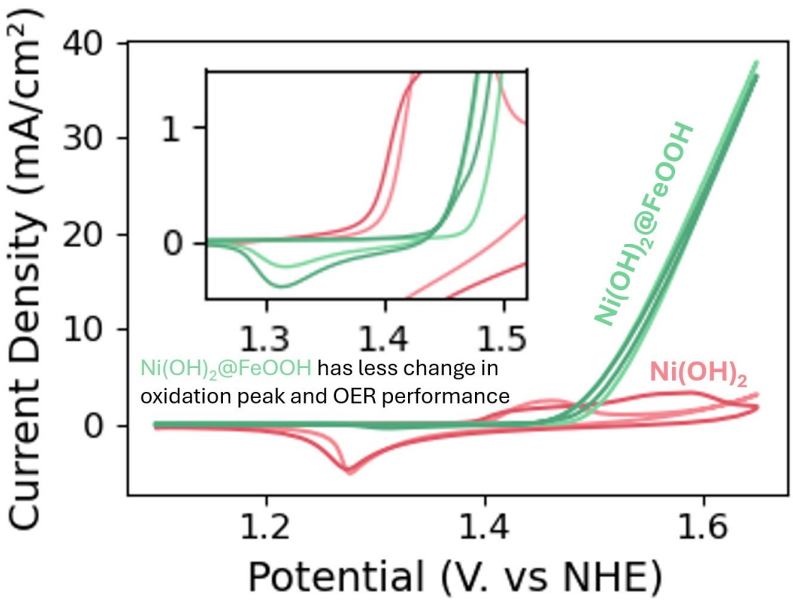

Fig. S23 Cyclic Voltammetry of $Ni(OH)_2$ and $Ni(OH)_2$@FeOOH compares their stability
The cyclic voltammetry of $Ni(OH)_2$ reveals that the redox peak of $Ni(OH)_2$ changes dramatically after 10 cycles, which suggests its structure changes dramatically, and the OER performance decreases significantly. As a comparison, the redox peak and OER performance of $Ni(OH)_2$@FeOOH have minor changes after 10 cycles, meaning it's relatively stable compared to $Ni(OH)_2$.

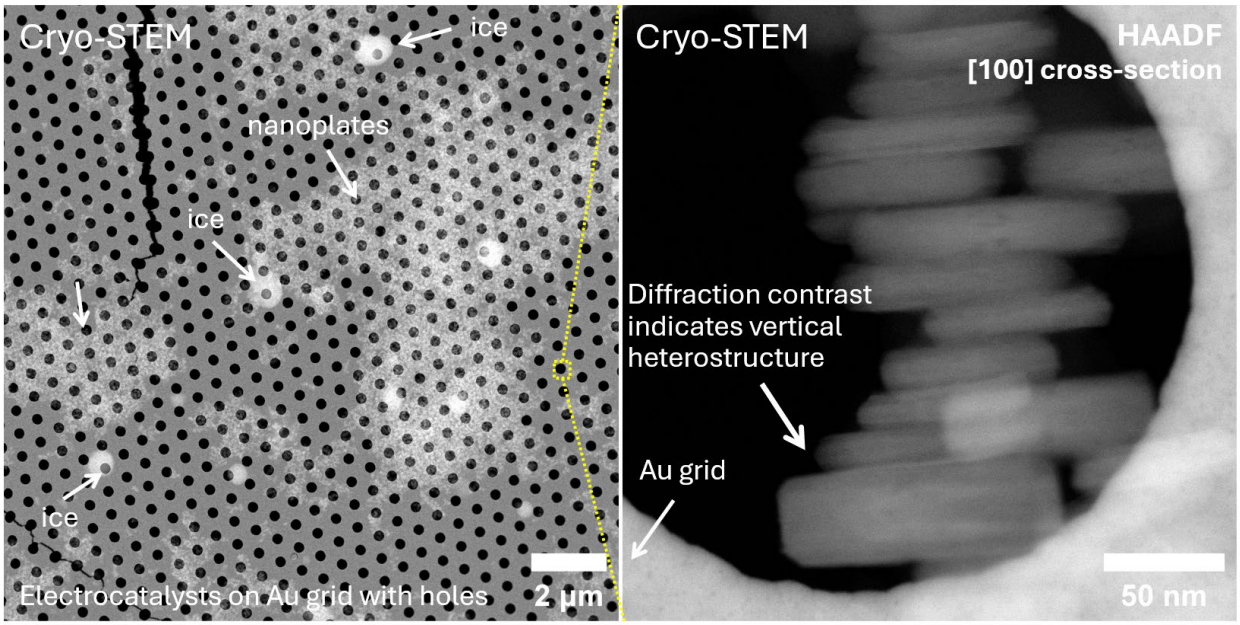

Fig. S24 Cryo-STEM HAADF image of $Ni(OH)_2$@FeOOH in large field-of-view
Cryo-STEM HAADF image of $Ni(OH)_2$@FeOOH on HexAuFoil grid, shows the ice and nanoplates on the Au foil with circular hole arrays. In the hole arrays, we can observe a stack of $Ni(OH)_2$@FeOOH nanoplates, and the diffraction contrast reveals their vertical heterostructure after the OER reaction.

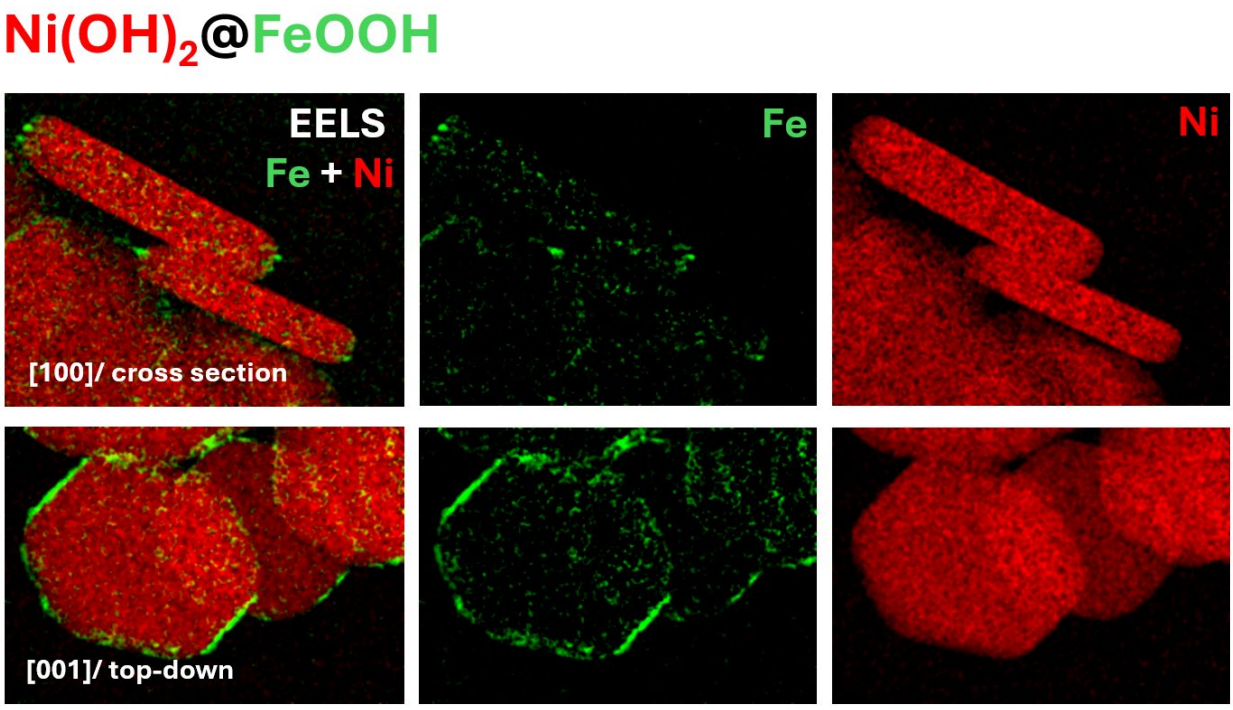

Fig. S25 Cryo-STEM EELS image of $Ni(OH)_2$@FeOOH
STEM EELS mapping of Ni and Fe and simultaneous ADF in $Ni(OH)_2$@FeOOH along both [100] side and [001] top-down view, showing that the Fe is still only selectively distributed on the edge plane of $Ni(OH)_2$.

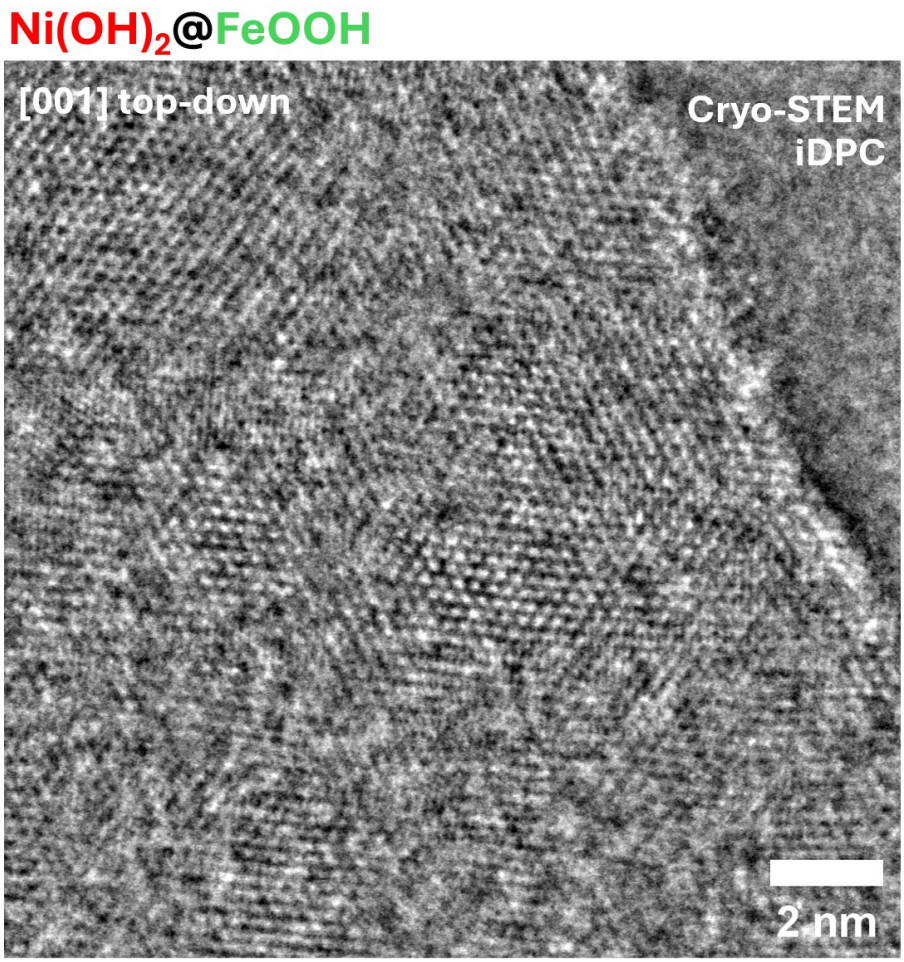

Fig. S26 Cryo-STEM iDPC image of $Ni(OH)_2$@FeOOH from top-down view

Atomic resolution Cryo-STEM iDPC image of $Ni(OH)_2$@FeOOH from top-down view shows a certain degree of disorder in $Ni(OH)_2$@FeOOH. Since after the OER reaction, the core of $Ni(OH)_2$@FeOOH forms a NiOOH@$Ni(OH)_2$@NiOOH vertical heterostructure, and the iDPC image here is a projection along the vertical heterostructure, it's impossible to analyze the vertical heterostructure along the vertical beam direction.

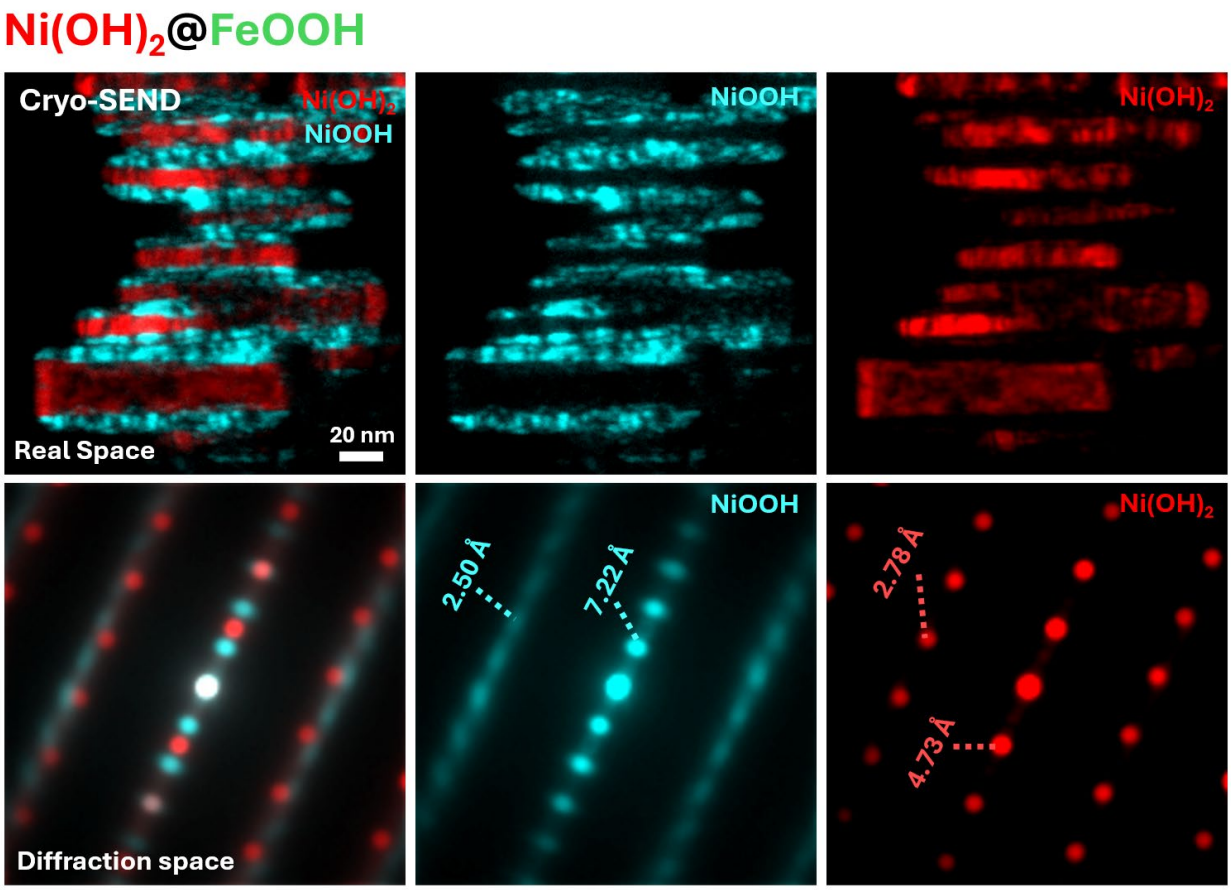

Fig. S27 Cryo-SEND of vertically stacked $Ni(OH)_2$@FeOOH nanoplates reveals a universal NiOOH@$Ni(OH)_2$@NiOOH vertical heterostructure after cycling

Cryo-scanning electron nanodiffraction (Cryo-SEND) imaging of multiple $Ni(OH)_2$@FeOOH nanoplates demonstrates that the formation of a vertical NiOOH@$Ni(OH)_2$@NiOOH heterostructure within the core is a universal feature after electrochemical cycling. In real-space mapping, different colors represent the spatial distribution of NiOOH and $Ni(OH)_2$, revealing that each nanoplate retains $Ni(OH)_2$ in the bulk, sandwiched by NiOOH layers on the top and bottom surfaces. The corresponding diffraction patterns, shown in matching colors, further confirm the structural identity: NiOOH is characterized by a 7.22 Å interlayer spacing and a 2.50 Å in-plane Ni–Ni distance. The diffraction spots appear blurred, reflecting their disordered structure. $Ni(OH)_2$, in contrast, displays sharp and symmetric diffraction spots, with a 4.73 Å interlayer spacing and a 2.78 Å in-plane Ni–Ni distance, consistent with its well-ordered crystalline nature.

Reference

1. Sac-Epée, N., Palacìn, M. R., Delahaye-Vidal, A., Chabre, Y. & Tara⁁scon, J.-M. Evidence for Direct γ - NiOOH ↔ β - Ni (OH) 2 Transitions during Electrochemical Cycling of the Nickel Hydroxide Electrode. *J. Electrochem. Soc.* **145**, 1434 (1998).
2. Ma, R., Liang, J., Liu, X. & Sasaki, T. General Insights into Structural Evolution of Layered Double Hydroxide: Underlying Aspects in Topochemical Transformation from Brucite to Layered Double Hydroxide. *J. Am. Chem. Soc.* **134**, 19915–19921 (2012).
3. M. Hunter, B., Hieringer, W., R. Winkler, J., B. Gray, H. & M. Müller, A. Effect of interlayer anions on [NiFe]-LDH nanosheet water oxidation activity. *Energy & Environmental Science* **9**, 1734–1743 (2016).
4. Dionigi, F. *et al.* In-situ structure and catalytic mechanism of NiFe and CoFe layered double hydroxides during oxygen evolution. *Nat Commun* **11**, 2522 (2020).
5. Sestu, M., Carta, D., Casula, M. F., Corrias, A. & Navarra, G. Novel interpretation of the mean structure of feroxyhyte. *Journal of Solid State Chemistry* **225**, 256–260 (2015).
6. Zeng, R. *et al.* Origins of enhanced oxygen reduction activity of transition metal nitrides. *Nature Materials* **23**, 1695–1703 (2024).
7. Zhitova, E. S., Krivovichev, S. V., Pekov, I. & Greenwell, H. C. Crystal chemistry of natural layered double hydroxides. 5. Single-crystal structure refinement of hydrotalcite, [Mg6Al2(OH)16](CO3)(H2O)4. *Mineralogical Magazine* **83**, 269–280 (2019).